ACS Catalysis

Research Article

pubs.acs.org/acscatalysis

# Mechanistic Studies of Electrode-Assisted Catalytic Oxidation by Flavinium and Acridinium Cations

Xin Yang,[†] Janitha Walpita,[†] Ekaterina Mirzakulova,[†] Shameema Oottikkal,[‡] Christopher M. Hadad,[‡] and Ksenija D. Glusac*,[†]

[†]Department of Chemistry, Center for Photochemical Sciences, Bowling Green State University, Bowling Green, Ohio 43403, United States

[‡]Department of Chemistry, The Ohio State University, Columbus, Ohio 43210, United States

Supporting Information

**ABSTRACT:** Electrochemical behavior of flavinium (Et-Fl$^+$) and acridinium (Acr$^+$) cations is presented, in order to investigate their activity toward catalytic water oxidation. Cyclic voltammograms of Acr$^+$ and Et-Fl$^+$ in acetonitrile are qualitatively similar, with oxidation peaks at highly positive potentials, and these oxidation peaks depend strongly on the type of the working electrode being used. However, the two model compounds exhibit different behaviors in the presence of water: while Et-Fl$^+$ facilitates electrocatalytic water oxidation through an electrode-assisted mechanism, water oxidation is not accelerated in the presence of Acr$^+$. A comparative study of variable scan-rate cyclic voltammetry, concentration dependence, and spectroelectrochemical behavior of two model compounds suggest that Et-Fl$^+$ and Acr$^+$ exhibit different reaction pathways with the electrode surface. On the basis of the experimental results, a mechanism is proposed to account for the observed differences in electrocatalysis.

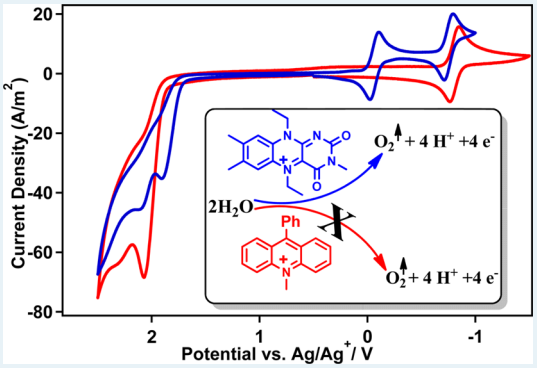


**KEYWORDS:** *electrocatalytic water oxidation, iminium ions, electrode-assisted, pseudobase, electron transfer*

## INTRODUCTION

Electrocatalytic oxidation of water to oxygen[1−6] is one of the key processes that needs to be improved for the development of efficient solar fuel cells.[7,8] To avoid high-energy intermediates, such as hydrogen peroxide and hydroxyl radical, water oxidation needs to occur via a simultaneous, proton-coupled four-electron transfer process ($2H_2O \rightarrow O_2 + 4H^+ + 4e^-$).[9] This requirement for synchronicity poses substantial challenges in the development of catalysts that evolve oxygen from water at sufficiently low overpotentials. The low catalytic overpotential can only be achieved if all four one-electron oxidation steps in the water oxidation pathway exhibit the same change in free energy,[10] which is a tall order to fill. Even if high-energy intermediates are avoided, water oxidation is significantly thermodynamically uphill and requires large potentials ($E^\circ$ = +1.23 V vs NHE), causing most molecular catalysts to undergo other unwanted chemical reactions (oxidative damage). In an attempt to overcome these challenges, a great scientific effort is aimed at studies of well-defined molecular water-oxidation catalysts, whose mechanistic details can be readily investigated using available spectroscopic techniques.[11−25]

Most of the currently known oxygen-evolving molecular catalysts are complexes made of second and third row transition metals, such as Ru and Ir.[24,26−47] Due to extensive mechanistic studies of model Ru-based bimetallic catalysts,[27−34] notable progress in the field occurred since the discovery of the first molecular catalyst in 1982.[26] For example, the key O−O bond formation of the Ru blue dimer is currently thought to occur via a nucleophilic attack of water to the Ru$^V$=O species to form a hydroperoxyl intermediate.[28,29] Furthermore, significant improvement in the catalyst's stability was achieved by the discovery of new model Ru-based catalysts that exhibit a single metallic site.[24,35−41] While some of these monometallic catalysts oxidize water via the monomolecular mechanism involving the above-mentioned nucleophilic attack of water to the Ru$^V$=O intermediate, the complexes discovered by Sun appear to undergo a bimolecular O−O bonding mechanism, in which a Ru−O−O−Ru peroxide is made by a radical coupling mechanism.[24] More recently, mononuclear iridium complexes have been reported to efficiently catalyze water oxidation.[42−44] However, it is important to note that some of the Ir-based catalysts were found to undergo ligand oxidation to form iridium oxides that are highly active toward water oxidation.[45−47]

Received: April 17, 2014
Revised: June 12, 2014
Published: June 30, 2014

   dx.doi.org/10.1021/cs5005135 | ACS Catal. 2014, 4, 2635−2644

Inspired by the catalytic water oxidation in natural photosynthetic centers,[2] a large scientific effort was dedicated to the studies of model manganese complexes.[16,19−21,48,49] However, these studies have shown that the manganese complexes are unstable outside the protein environment and that only a few complexes were found to be catalytically active.[21,50,51] Most of these catalysts, except for the recent report by Åkermark,[51] required a sacrificial oxidant as an oxygen-atom donor.[21,50] Even though Mn-based molecular catalysts are scarce, significant research progress was achieved recently using other first-row transition metal complexes, such as Fe, Co, and Cu-based catalysts.[11−16,52−56]

Our group is interested in organocatalytic molecular frameworks for oxygen evolution.[57,58] Fully organic water oxidation catalysts have not been reported in the literature, likely due to the chemical instability of organic compounds under strongly oxidizing conditions required for water oxidation. Despite this disadvantage, organic catalysts should not be neglected, since they offer some advantages over the currently known molecular systems: (i) There are fewer concerns about limited resources, as the organic molecules are made of earth-abundant elements (C, H, O, and N). (ii) Synthetic organic chemistry is a mature field, offering easy access to a wide variety of molecular motifs for catalysis. (iii) Organic catalysts are likely to be less toxic than the metal-containing analogs.

We recently found that a simple flavinium ion (Et-Fl$^+$, Scheme 1) facilitates the electrocatalytic water oxidation at high overpotentials.[59] This preliminary study provided two key mechanistic insights regarding the catalysis: (i) the hydroxylated flavin FlOH$^+$ was identified as a likely catalytic intermediate using UV/vis spectroelectrochemical measurements, and (ii) the surface of the working electrode plays an important role in catalysis (the electrocatalytic current was observed on glassy carbon (GC) and platinum (Pt) electrodes, while no catalysis was observed in the case of the fluoride-doped tin oxide (FTO) electrode).

**Scheme 1. Structures of N(5)-Ethylflavinium Perchlorate (Et-Fl$^+$) and *N*-Methyl-9-phenylacridinium Perchlorate (Acr$^+$)[a]**

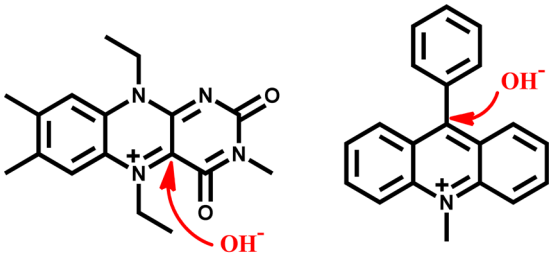


Et-Fl$^+$ Acr$^+$

[a]The red arrows show the sites where hydroxide attack occurs to generate the corresponding pseudobase derivatives Et-FlOH and AcrOH.

In an attempt to identify which functional groups of Et-Fl$^+$ are responsible for the catalytic activity, we investigate here the electrochemical behavior of a structurally similar, but significantly simpler, derivative: *N*-methyl-9-phenylacridinium perchlorate (Acr$^+$, Scheme 1). This manuscript describes the electrochemical behavior of Acr$^+$ and contrasts it to that of Et-Fl$^+$. The results of our study suggest that, even though some similarities are found in the electrochemical behaviors of Et-Fl$^+$ and Acr$^+$, the acridinium ion does not facilitate the electrocatalytic oxidation of water to oxygen. A plausible mechanistic explanation of these differences is presented.

## EXPERIMENTAL SECTION

**Methods.** All chemicals were purchased from commercial suppliers and used without further purification. $^1$H and $^{13}$C NMR spectra were recorded on a Bruker Avance 300 MHz system. GC-MS spectra were measured on a Shimadzu GC-MS-Q5050A spectrometer. UV/vis absorption spectra were recorded on an Agilent 8453 UV Spectrophotometer in a 1 cm quartz cell. 10-Methyl-9-phenylacridinium perchlorate (Acr$^+$) was purchased from TCI America. Et-Fl$^+$ was synthesized according to the previously published procedure.[57]

**Cyclic Voltammetry.** Cyclic voltammetry was performed using a BASi epsilon potentiostat in a VC-2 voltammetry cell (Bioanalytical Systems) using glassy carbon (3 mm diameter, MF-2012, Bioanalytical Systems), fluorine-doped tin oxide FTO (area 4.5 cm$^2$, Hartford Glass), boron-doped diamond BDD (area 2 cm$^2$, Fraunhofer USA), and Pt (1.6 mm diameter, MF-2013, Bioanalytical Systems) working electrodes; a platinum wire auxiliary electrode (MW-4130, Bioanalytical Systems); and a nonaqueous Ag/Ag$^+$ reference electrode (MF-2062, Bioanalytical Systems). Acetonitrile was purchased from Sigma-Aldrich (anhydrous, 99.8%) and purified by reflux over $CaH_2$ for 8 h, followed by distillation. Tetrabutylammonium perchlorate (TBAP) was purchased from Sigma-Aldrich, recrystallized from methanol, and dried under a vacuum. Electrochemical potentials were referenced to NHE by adding 0.548 V to the experimental potentials.[60]

**Bulk Electrolysis.** Bulk electrolysis was performed in a custom-designed two-compartment gastight electrochemical cell under an argon atmosphere. One arm of the cell contained (i) a Pt electrode (0.25″ × 4″, Home Science Tools), (ii) a Ag/AgCl aqueous reference electrode (Bioanalytical Systems), (iii) an oxygen sensor (FOXY-R, Ocean Optics), (iv) a Schlenk line outlet connected to a round-bottom flask, (v) a gas inlet. The second arm contained a Pt wire as an auxiliary electrode and a gas outlet port. Electrolysis was carried out using an EC Epsilon potentiostat (BioanalyticalSystem) at +2.1 V vs Ag/AgCl in a 0.1 M phosphate buffer at different pH values. The water for electrolysis was deionized using a water purification system (Barnstead Nanopure System). Prior to each experiment, the sensor was calibrated using a two-point reading (20.9% $O_2$ in the air and 0% $O_2$ in the argon-purged cell). An empty cell was degassed with argon for 2 h. In parallel, a prepared solution of 1.5 mM Acr$^+$ in the phosphate buffer at pH = 2, 7, and 11 was purged by argon in a round-bottom flask connected to the cell by a Schlenk connector. The Acr$^+$ solution was then transferred to the cell through a Schlenk connection. The oxygen sensor probe was placed in the headspace, and data were collected at 10 s intervals. Before electrolysis was initiated, the $O_2$ signal was monitored for 10 min to ensure there was no leakage of $O_2$ from the air outside the cell. After ensuring there were no leaks, the electrolysis was initiated and continued for 2 h. Conversion of %$O_2$ into micromoles was obtained from the known volumes of the solution ($V_S$ = 100 mL) and the headspace ($V_H$ = 70 mL) using Henry's Law.

**Spectroelectrochemistry.** UV/vis spectroelectrochemistry was done using a Pt mesh working electrode, nonaqueous Ag/Ag$^+$ reference, and Pt wire as an auxiliary electrode, and the absorption spectra were recorded on a HP 8453 UV/vis


dx.doi.org/10.1021/cs5005135 | ACS Catal. 2014, 4, 2635−2644

spectrophotometer. The spectroelectrochemical cell was purchased from Bioanalytical Systems (EF-1350). A solution of 1 mM $Acr^+$ in acetonitrile containing 0.1 M TBAP was degassed with argon prior to each experiment. The changes in the absorption were monitored in 6 s intervals after applying a potential of +2.7 V vs NHE. In addition, the chemical oxidation of 1.0 mM AcrOH solution was performed with 1.5 mM $Cu(ClO_4)_2 \cdot 6H_2O$ in acetonitrile, and the UV/vis absorption spectra were recorded as a function of time.

**Computational Methods.** All geometries were optimized using Becke's three-parameter hybrid exchange functional with the Lee–Yang–Parr correlation functional (B3LYP) method,[61,62] along with other DFT functionals (S2, Supporting Information), with the 6-311++G** basis set in the Gaussian 09 suite of software.[63] All stationary points were verified to be minima by harmonic vibrational frequency calculations. In order to estimate the effect of solvation, polarizable continuum model (PCM) calculations for acetonitrile as a solvent and its effect on the oxidation potential were calculated with respect to NHE at +4.4 V.[64]

## RESULTS AND DISCUSSION

**1. Model Compounds.** The aim of this study is to pinpoint the structural motifs of $Et\text{-}Fl^+$ that are responsible for its electrocatalytic activity. For this purpose, an investigation of a significantly simpler model compound $Acr^+$ (Scheme 1) is presented. While $Et\text{-}Fl^+$ exhibits a number of functional groups, $Acr^+$ contains only the aromatic iminium ion moiety as a possible site for electrocatalysis. The iminium ion $Acr^+$ forms the pseudobase intermediate AcrOH in basic solution (Figure 1). This is an important property, since our previous study of

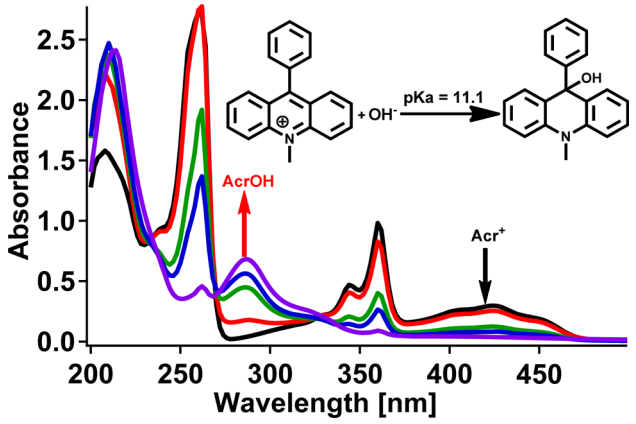


**Figure 1.** UV/vis absorption spectra of $Acr^+$ in acetonitrile/water = 1000:1 mixture at varying pH values: pH 7 (black), 10.4 (red), 11.1 (green), 11.3 (blue), and 12.3 (purple).

$Et\text{-}Fl^+$ electrochemistry[59] identified the intermediate $Et\text{-}FlOH^+$ as a plausible intermediate in catalysis. On the other hand, pseudobase formations from $Et\text{-}Fl^+$ and $Acr^+$ differ in two significant ways: (i) Et-FlOH formation occurs more readily (pseudobase $pK_a$ = 3.5)[59] than the formation of AcrOH (pseudobase $pK_a$ = 11.1, Figure 1); (ii) the hydroxide ion attaches in the 4-position of $Acr^+$, while the 2-hydroxy product is formed in the case of $Et\text{-}Fl^+$ (Scheme 1). Thus, $Acr^+$ resembles $Et\text{-}Fl^+$ only by the presence of iminium ion/pseudobase equilibrium. This manuscript compares the electrochemical behavior of the two model compounds: the first part of the text addresses their similarities, and the second section reports the important differences between them.

**2. $Et\text{-}Fl^+$ vs $Acr^+$: Similarities.** *2.1. Cyclic Voltammetry.* The cyclic voltammogram of $Acr^+$ in acetonitrile is qualitatively very similar to that of $Et\text{-}Fl^+$ (Figure 2). The reversible one-

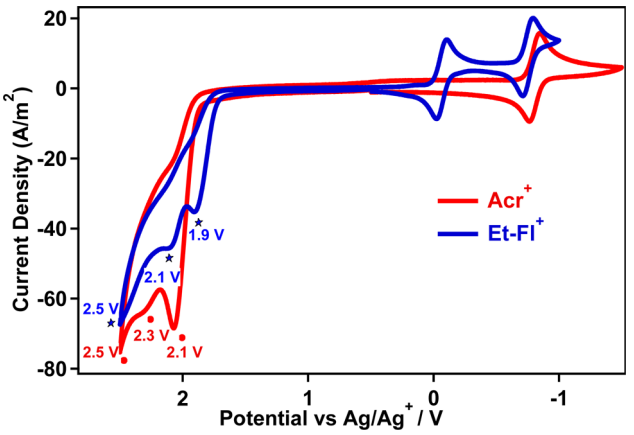


**Figure 2.** Cyclic voltammograms of 2 mM $Acr^+$ (red) and 2 mM $Et\text{-}Fl^+$ (blue) in acetonitrile (electrolyte: TBAP). Scan rate: 100 mV/s. Electrodes: platinum working electrode, platinum counter electrode, nonaqueous $Ag/Ag^+$ reference electrode.

electron reduction of $Acr^+$ to generate neutral $Acr^\bullet$ radical appears at −0.9 V vs $Ag/Ag^+$, which is consistent with literature reports.[65] At positive potentials, three oxidation peaks were observed in the presence of $Acr^+$ and $Et\text{-}Fl^+$ (red circles and blue stars in Figure 2). Importantly, an increase in the current is observed at potentials above +2 V (vs $Ag/Ag^+$), which is in the case of $Acr^+$ shifted by ∼0.2 V to a more positive potential relative to the corresponding peak of $Et\text{-}Fl^+$. These results suggest that $Acr^+$ exhibits similar oxidation behavior to $Et\text{-}Fl^+$.

Since the oxidation behavior of $Et\text{-}Fl^+$ was previously shown to strongly depend on the type of the working electrode used in the experiment,[59] the effect of the working electrode was investigated for $Acr^+$ as well (Figure 3). The electrodes used in this study are as follows: platinum (Pt), glassy carbon (GC),

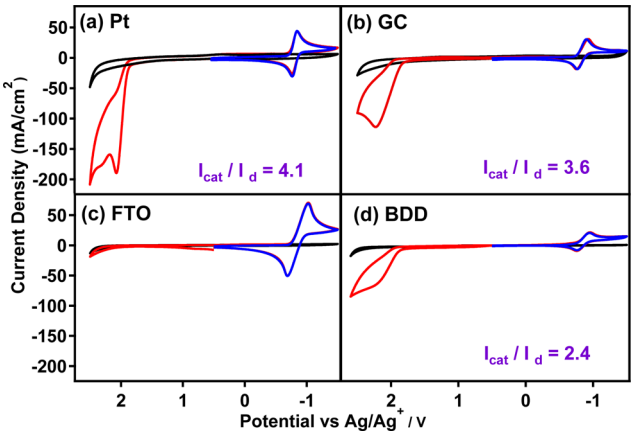


**Figure 3.** Cyclic voltammograms of 2 mM $Acr^+$ in acetonitrile containing 0.1 M TBAP at the (a) Pt electrode, (b) GC electrode, (c) FTO electrode, (d) BDD electrode (scan rate: 100 mV/s). Scan direction: blue curve, +0.5 → −1.5 → +0.5 V; red curve, +0.5 → +2.5 → −1.5 → +0.5 V. Black curve shows a baseline scan. $I_{cat}/I_d$ is the ratio of currents at +2 and −1.0 V.


dx.doi.org/10.1021/cs5005135 | ACS Catal. 2014, 4, 2635–2644

fluoride-doped tin oxide (FTO), and boron-doped diamond (BDD) electrode. These electrodes were selected because they exhibit substantially different surface chemistry.[66] As shown in Figure 3, the reduction potential of $Acr^+$ does not depend on the type of the electrode used (reduction occurs at −0.9 V vs $Ag/Ag^+$ for all four electrodes), which is indicative of an outer-sphere electron-transfer process.[67] In contrast, the oxidation potential and current density of $Acr^+$ is strongly electrode-dependent: the current above 1.9 V is observed on Pt, GC, and BDD electrodes, while no oxidation was observed on the FTO electrode. These electrochemical results are consistent with those observed previously in cyclic voltammograms of Et-$Fl^+$.[59] The strong effect of the working electrode on the anodic oxidation of $Acr^+$ and Et-$Fl^+$ suggest that these iminium cations interact with the electrode surface prior to the charge transfer (inner-sphere electron transfer mechanism).[67]

The current observed at ∼2 V decreases in the following order of working electrodes: Pt > GC > BDD > FTO, as can be deduced from the $I_{cat}/I_d$ ratios reported in Figure 3. Thus, $Acr^+$ and Et-$Fl^+$ interact most efficiently with the platinum electrode and least efficiently with the FTO electrode. This electrode-dependent behavior has prompted us to determine computationally the standard potentials for $Acr^+$ and Et-$Fl^+$ in acetonitrile using the previously developed DFT (density functional theory, B3LYP) methodology[68] (Table 1, more information is available in section S2, Supporting Information). For comparison purposes, the experimental and calculated potentials were also obtained for $NMe_2$-$Acr^+$, which exhibits a simple outer-sphere one-electron oxidation at 1.32 V (Figure S2, Supporting Information). The results show that the calculated potentials for Et-$Fl^+$ ($E_{Et\text{-}Fl^+}$ = 2.44 V) are very close to the experimentally observed anodic potentials on the Pt working electrode ($E_{Et\text{-}Fl^+}$ = 2.40 V). However, the calculated potential for $Acr^+$ (2.02 V) is much lower than the experimentally determined value (2.60 V). We have repeated calculations of oxidation potential using different DFT functionals (S2, Supporting Information), but the calculated data show a lower oxidation potential for $Acr^+$ than the experimentally determined potential. On the basis of the calculated $Acr^+$ potential (2.02 V), we conclude that the experimental one-electron oxidation of $Acr^+$ occurs with slow kinetics, even when the Pt working electrode is used (2.60 V). This large difference in the calculated and experimental potentials suggests that the interaction of $Acr^+$ with the surface of the Pt electrode is not sufficiently strong to provide fast charge transfer kinetics. On the other hand, a good match between the calculated and experimental oxidation potentials of Et-$Fl^+$ implies a stronger interaction of Et-$Fl^+$ with the Pt surface.

Even though cyclic voltammograms of $Acr^+$ show a strong dependence on the working electrode material, this interaction between $Acr^+$ and the electrode's surface appears to be transient: the baseline cyclic voltammogram collected using the working electrode that was previously kept in the $Acr^+$ solution under an applied potential of 2.1 V for 10 min showed no presence of any electrochemically active species adsorbed on the electrode's surface (Figure S1, Supporting Information).

The question that remains unanswered is, what type of interaction between $Acr^+$/Et-$Fl^+$ and the electrode's surface exists to cause the observed trend? The adsorption of organic molecules to surfaces of several types of electrodes was observed previously, and the adsorption characteristics were found to strongly depend on the applied potential.[69−71] For example, pyridine-based derivatives form flat adsorbates at negative potentials (due to $\pi$ interactions), while the perpendicular orientation is preferred at high potentials (via nitrogen lone pairs interactions).[72] In the case of $Acr^+$ and Et-$Fl^+$, the nitrogen centers are alkylated, so the lone pair interactions between these molecules and the electrode's

**Table 1. Calculated (B3LYP/6-311++G**, with PCM (Acetonitrile) As Solvent) and Experimental Oxidation Potentials of Et-$Fl^+$ and $Acr^+$ in Acetonitrile**

| | oxidation potential vs NHE (V) | |
|---|---|---|
| compounds | calculation | experiment |
| Et-$Fl^+$ | 2.44 | 2.40[a] |
| $Acr^+$ | 2.02 | 2.60[a] |
| $Me_2N$-$Acr^+$ | 1.32 | 1.30 |

[a]Anodic peak potentials for irreversible signals on Pt working electrode.

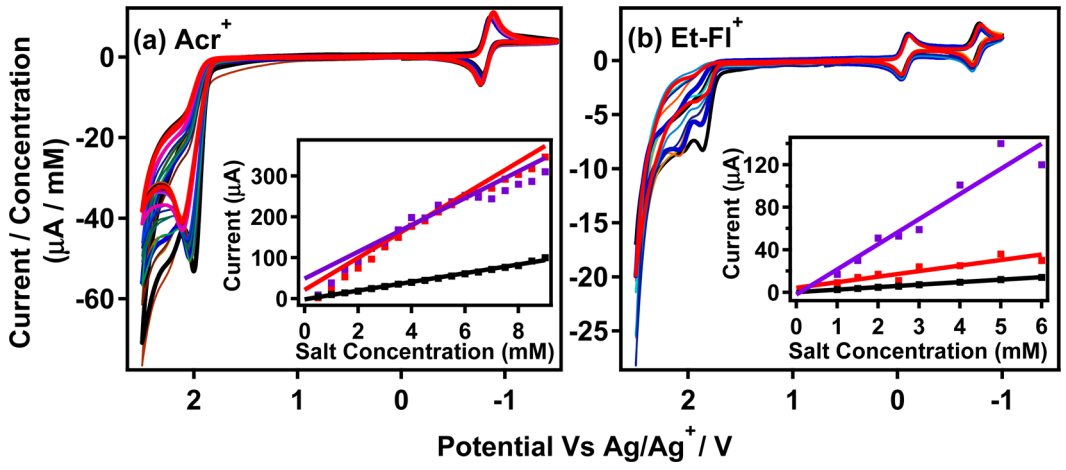


**Figure 4.** Cyclic voltammograms of (a) $Acr^+$ and (b) Et-$Fl^+$ at different concentrations: 1 mM (black), 2 mM (brown), 3 mM (light blue), 4 mM (green), 5 mM (dark blue), 6 mM (pink), 7 mM (purple), 8 mM (orange), 9 mM (red). Inset: Plot of current vs salt concentration at 2.1 V (purple line), 2.5 V (red line), and the corresponding reduction potentials (−0.1 V for Et-$Fl^+$ and −1.0 V for $Acr^+$ (black line); scan rate: 100 mV/s, Pt working electrode).


dx.doi.org/10.1021/cs5005135 | ACS Catal. 2014, 4, 2635−2644

surface are not possible. On the other hand, the $\pi$ interactions with the electrode surface are a plausible mode of adsorption in the case of $Acr^+$ and Et-$Fl^+$, since the strong interactions between positively charged organic molecules and the surface of the gold electrode were observed at positive potentials.[71]

Previous studies suggest that all four electrodes generate hydroxylated surface S−OH species, where S is the electrode's surface. The hydroxylated species on Pt and GC electrodes are considered to be "active," as they tend to undergo further oxidation to generate S−O species.[66] On the other hand, BDD and FTO electrodes are considered to be "inactive," as they do not undergo additional oxidation steps. Thus, it appears that the catalytic current observed for $Acr^+$ and Et-$Fl^+$ is stronger on electrodes that are known to generate S−O species. On the basis of these findings, we hypothesize that $Acr^+$ and Et-$Fl^+$ selectively interact with S−O species, which causes the observed trend of current decrease from Pt to the FTO electrode. However, further spectroscopic studies are needed to address the structure of adduct formed between these iminium ions and the surface of the electrode.

It is interesting to mention that the Ru-based blue dimer is also catalytically inactive on an ITO (indium−tin oxide) electrode,[73] which exhibits similar electrochemical behavior as the FTO electrode. The catalysis by the blue dimer was observed on the ITO electrode in the presence of an electron mediator. Similarly, we find that the oxidation peak of $Acr^+$ appears on the FTO electrode when ferrocene is used as an electron mediator (Figure S6, Supporting Information). These results indicate that the anodic current increase is absent for iminium ions on the FTO electrode due to slow electron transfer kinetics, and that this charge transfer process can be accelerated by the addition of an electron transfer mediator. The fact that Pt and GC electrodes do not require an electron transfer mediator suggests that iminium ions interact with the surfaces of Pt and GC electrodes in a way that facilitates the electron transfer process.

*2.2. Concentration Dependence.* An almost linear dependence of the current on the iminium ion concentration suggests that the rate-determining step of the process at potentials above +1.9 V is monomolecular with respect to $Acr^+$ and Et-$Fl^+$ (red and purple-colored lines in inset plots of Figure 4). However, a closer inspection of the cyclic voltammograms (Figure 4) shows that the anodic peaks of both $Acr^+$ and Et-$Fl^+$ undergo shape and intensity changes at increasing concentrations. While the one-electron reduction peaks of $Acr^+$ at −0.9 V and Et-$Fl^+$ at +0.1 V are almost identical (once the currents are scaled to account for different iminium ion concentrations by plotting $I/c$ on the $y$ axis), the oxidation peaks show different behavior: (i) the $Acr^+$ peak at +1.9 V and Et-$Fl^+$ peaks at +1.7 and +2.1 V undergo a decrease in the peak current, and the peak potentials shift to more positive values at higher concentrations. These results indicate that the electrochemical reaction is more efficient at lower concentrations of the iminium ion, possibly due to the fact that the catalysis is limited by the availability of the oxide sites on the electrode's surface.

## 3. Et-$Fl^+$ vs $Acr^+$: Differences.

*3.1. Water Addition.* Despite the similarities between Et-$Fl^+$ and $Acr^+$ presented in the previous section, the two iminium ions exhibit different behavior in the presence of water. While the addition of water to the acetonitrile solution of Et-$Fl^+$ gives rise to an increase in the current at potentials above +2 V,[59] the $Acr^+$ solution is not affected (Figure 5). The cyclic voltammograms of $Acr^+$ on Pt and GC electrodes (Figure 5b and d) exhibit only a modest

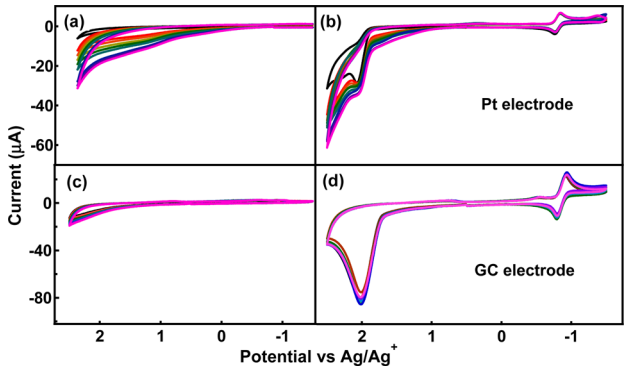


**Figure 5.** Cyclic voltammograms of 2 mM $Acr^+$ in acetonitrile with varying concentrations of pH 7 water (0, 50, 100, 150, 200, 250, 300, 350, 400, and 450 mM) at Pt (b) and GC (d) electrodes. The corresponding baseline scans are shown in panels a and c for Pt and GC electrodes, respectively. Sweep rate: 100 mV/s. Scan direction: +0.5 → +2.5 → −1.0 → +2.5 V.

increase in the current above +2 V, which is equivalent to the increase in the background current (Figure 5a and c) due to water oxidation by the working electrodes. Thus, even though an increase in the current at ∼2 V is observed in the presence of $Acr^+$ and maintained in the presence of water, this process does not facilitate the electrocatalytic water oxidation. The opposite behavior was observed for Et-$Fl^+$, where increasing concentration of water caused a significant increase in the current at potentials above +2 V.

*3.2. Bulk Electrolysis.* Additional evidence that $Acr^+$ does not facilitate electrocatalytic water oxidation is obtained from the controlled potential electrolysis (Figure 6). The oxygen

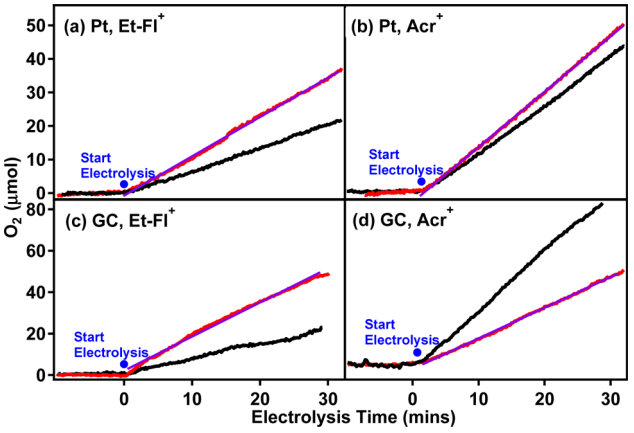


**Figure 6.** Oxygen evolution during controlled potential electrolysis at +2.1 V vs Ag/AgCl of 0.1 M aqueous phosphate solution in the presence (red) and absence (black) of 1.5 mM iminium ions. The purple line in each panel represents the $O_2$ evolution calculated from the faradaic efficiencies (FE) reported below. (a) Et-$Fl^+$, pH = 2, FE: 70%, Pt working electrode. (b) $Acr^+$, pH = 11, FE: 55%, Pt electrode. (c) Et-$Fl^+$, pH = 2, FE: 35%, GC electrode. (d) $Acr^+$, pH = 11, FE: 45%, GC electrode.

evolution was measured during controlled potential electrolysis at 2.1 V vs Ag/AgCl in aqueous $Acr^+$ and Et-$Fl^+$ solutions. In the absence of iminium ions, oxygen evolution was observed due to electrocatalytic water oxidation by the working electrodes (GC and Pt, black curves in Figure 6). In the presence of $Acr^+$, a negligible increase in the oxygen evolution can be observed relative to the blank in the case of the Pt


dx.doi.org/10.1021/cs5005135 | ACS Catal. 2014, 4, 2635−2644

electrode, while a significant decrease was observed for the GC electrode (red curves, Figure 6b and d). Compared to $Acr^+$, electrolysis of aqueous Et-$Fl^+$ solution gave rise to a noticeable increase in the oxygen relative to the blank scans (Figures 6a and c), which is consistent with our previous report.[59]

Thus, despite the fact that $Acr^+$ and Et-$Fl^+$ exhibit similar electrochemical behavior in a nonaqueous medium, these two compounds exhibit different behavior in the presence of water: while Et-$Fl^+$ facilitates electrocatalytic water oxidation, $Acr^+$ does not (even suppresses the process at the GC electrode). Since $Acr^+$ and Et-$Fl^+$ generate pseudobase derivatives at different pH values, we performed the experiments at two different pH values (pH = 2 for Et-$Fl^+$ and pH = 11 for $Acr^+$), in order to maintain the pH at values just below the corresponding pseudobase $pK_a$ values for the two systems. To investigate whether $Acr^+$ exhibits different behavior at other pH values, we performed the controlled potential electrolysis at other pH values (pH = 2 and 7). The results of this study showed that $Acr^+$ does not facilitate the oxygen evolution at either of these pH values (Figure S3, Supporting Information).

*3.3. Scan Rate Dependence.* The investigation of dynamics of the electrocatalytic process was attempted using scan-rate dependent cyclic voltammetry of Et-$Fl^+$ and $Acr^+$ in the 0.01 to 5 V/s range (Figure 7). At low scan rates (e.g., 30 mV/s), the

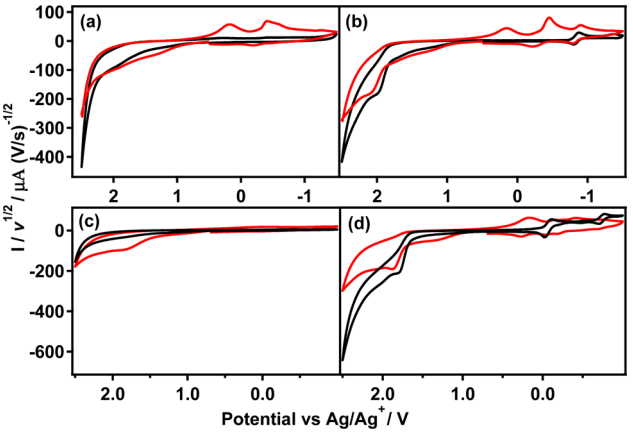


**Figure 7.** Scan rate dependent cyclic voltammograms of 1.5 mM $Acr^+$ (b) and 1.5 mM Et-$Fl^+$ (d) in acetonitrile with 450 mM water (pH = 7 for $Acr^+$ and pH = 2 for Et-$Fl^+$) at the Pt electrode. Corresponding baseline scans in the absence of iminium ions are shown in a for acetonitrile containing 450 mM pH = 7 water and c for acetonitrile containing 450 mM pH = 2 water. Scan rate: 30 mV/s (black), 500 mV/s (red). Electrolyte: TBAP.

current at potentials above +2 V is large, with baseline-subtracted $I_{cat}/I_d$ ratios reaching values above 20 (for $Acr^+$) and 8 (for Et-$Fl^+$). These results suggest that the low-scan rate provides sufficient time for the electrocatalysis to occur, as can be concluded by the recovery of the iminium ion reduction peaks in the reverse scan and absence of any additional reduction peaks. In contrast, the higher scan rates (e.g., 500 mV/s) lead to a decrease in the current above +2 V and the appearance of additional reduction peaks during the reduction scan, both of which suggest a loss of catalytic activity. For example, the return scan upon oxidation of $Acr^+$ at potentials above +2 V generates three reduction peaks, at +0.3, −0.6, and −0.9 V. While the reduction peak at −0.9 V is present at all scan rates and is assigned to the one-electron reduction of $Acr^+$, the peaks at +0.3 and −0.6 V are present only at higher scan rates, and their growth coincides with a decrease in the catalytic current intensity at +2 V. Thus, these two peaks are likely signatures of the species formed during catalysis, which can be observed at higher scan rates, when the rate of catalysis is slower than the rate of potential sweep. Similar peaks are observed in the case of Et-$Fl^+$: in addition to the two reversible one-electron reduction peaks at −0.15 and −0.75 V observed at all scan rates, the high scan rate (e.g., 500 mV/s) voltammograms exhibit two new peaks at +0.2 and −0.4 V.

Importantly, the same two peaks at +0.2/+0.3 and −0.4/−0.6 V are observed at higher scan rate voltammograms of the baseline. These peaks are particularly large in the presence of water at pH = 7 (Figure 7a), while they are barely noticeable in the presence of water at pH = 2 (Figure 7c). Similar peaks were observed during anodic oxidation of water on the platinum working electrode and are assigned to the reduction of surface oxides.[74,75] On the basis of these reports, we assign the peaks at +0.2 and −0.4 V to the reduction of surface oxides S−O and S−OH that are formed as intermediates during the anodic oxidation of water at the Pt working electrode. Since the loss of catalysis in baseline scans occurs at the same scan rates and with the same intermediates as in the presence of iminium ions, we conclude that the rate-determining step in electrode-assisted catalysis by iminium ions involves the reaction of surface oxides at the electrode's surface with iminium ions.

The scan-rate dependent voltammograms were analyzed using a model in which the reversible charge transfer is followed by a catalytic reaction, as follows:

$$I_m^+ \rightleftharpoons I_m^{2+} + e^- \quad k_{et} \tag{1}$$

$$I_m^{2+} + R \rightarrow I_m^+ + O \quad k_{cat} \tag{2}$$

where $I_m^+$ is one of the iminium ions (Et-$Fl^+$ or $Acr^+$) and R/O is the system being oxidized during catalysis (e.g., S−OH to S−O). The theory for the above model is well-known for cyclic voltammetry,[76] and the $k_{cat}$ values are usually estimated by obtaining the ratio of $I_{cat}/I_d$ as a function of $\nu^{-1/2}$ (where $I_{cat}$ is the current during catalysis, $I_d$ is the peak current for reversible electron transfer in the absence of the substrate R, and $\nu$ is the scan rate). A particularly simple relationship is obtained when the rate of catalysis is significantly higher than the scan rate: the current is directly proportional to $k_{cat}$ and independent of the scan rate. This limiting condition was used previously to evaluate rates of catalysis for other water oxidation catalysts.[56,77,78]

In the case of Et-$Fl^+$ and $Acr^+$ assisted catalysis, the limiting conditions were not achieved experimentally, likely due to small $k_{cat}$ values (even at very low scan rates, the current was still dependent on scan rate). Due to this complication, the estimates of $k_{cat}$ values were obtained by comparing our experimental $I_{cat}/I_d$ vs $\nu^{-1/2}$ plots with the plots simulated using the model presented in eqs 1 and 2 (simulation details are presented in section S4 of the Supporting Information). The experimental values for $I_{cat}$ were obtained by subtracting the baseline current obtained in the absence of iminium ions.

Both model compounds exhibit an increase in $I_{cat}/I_d$ values as the scan rate is decreased (increasing $\nu^{-1/2}$ values, Figure 8). At high scan rates ($\nu^{-1/2} \sim 0.45$ $(V/s)^{-1/2}$), the $I_{cat}/I_d$ values for Et-$Fl^+$ and $Acr^+$ are ~2, suggesting that iminium ions undergo a two-electron oxidation process prior to the rate-determining electrocatalytic step. At low scan rates ($\nu^{-1/2} = 22.3$ $(V/s)^{-1/2}$), the $I_{cat}/I_d$ ratios at +2.5 V increase to values of ~25 for $Acr^+$ and ~10 for Et-$Fl^+$, suggesting that the rate of the


dx.doi.org/10.1021/cs5005135 | ACS Catal. 2014, 4, 2635−2644

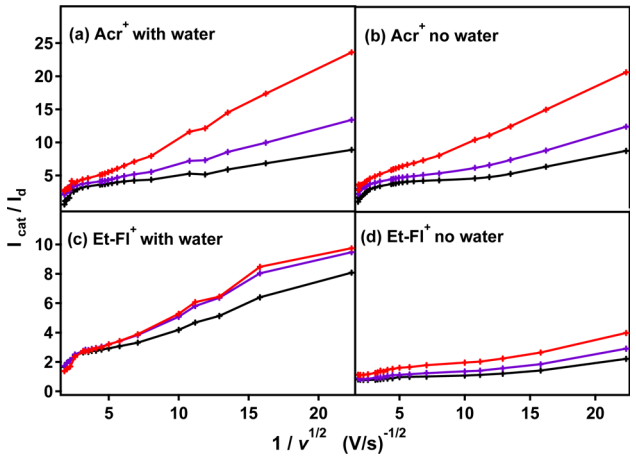


**Figure 8.** Baseline subtracted $I_{cat}/I_d$ ratios versus $\nu^{-1/2}$ at 2.1 V (black line), 2.3 V (purple line), and 2.5 V (red line) vs $Ag/Ag^+$. (a) $Acr^+$ in acetonitrile and 450 mM pH = 7 water mixture. (b) $Acr^+$ in acetonitrile. (c) Et-$Fl^+$ in acetonitrile and 450 mM pH = 2 water mixture. (d) Et-$Fl^+$ in acetonitrile (electrolyte: 0.1 M TBAP, Pt working electrode, $c$ = 1.5 mM).

electrocatalytic process is higher in the case of $Acr^+$. Despite faster electrocatalysis by $Acr^+$, this process is not affected by the presence of water: the $I_{cat}/I_d$ values are almost identical in the absence (Figure 8b) and presence (Figure 8a) of water. On the other hand, the $I_{cat}/I_d$ ratios of Et-$Fl^+$ (Figures 8c and d) are increased in the presence of water, particularly at 2.1 V potential. These results clearly indicate that $Acr^+$ and Et-$Fl^+$ catalyze two different electrochemical processes.

To evaluate the rate constants $k_{cat}$ for electrocatalysis by $Acr^+$ and Et-$Fl^+$, scan-rate dependent experiments were compared with the simulated data (Figure 9). The simulations were performed for $k_{cat}$ values in the 1−100 $s^{-1}$ range (Figure 9c), and the details of simulation are presented in the Supporting Information. The comparison of the experimental and the simulated $I_{cat}/I_d$ ratios suggest that $k_{cat}$ for electrocatalysis at 2.1 V by $Acr^+$ is ∼10 $s^{-1}$ and ∼1 $s^{-1}$ in the case of Et-$Fl^+$. Similar rate analysis was previously reported for the Ru-based catalyst by Meyer et al.,[77] where the $k_{cat}$ value was found to increase from 0.003 $s^{-1}$ in aqueous solution to a value of 1 $s^{-1}$ in a water−propylene carbonate solvent mixture. Even though $k_{cat}$ = 1 $s^{-1}$ observed for Et-$Fl^+$ is equivalent to that reported for the Ru-based catalyst, it is important to keep in mind that the two values were obtained at substantially different potentials (2.1 V vs $Ag/Ag^+$ in the case of Et-$Fl^+$ and 1.3 V vs $Ag/Ag^+$ in the case of Ru-based catalyst).[77]

*3.4. Spectroelectrochemistry.* Previous spectroelectrochemical studies on Et-$Fl^+$ provided valuable information regarding the intermediates formed during the electrocatalytic process.[59] For example, oxidation of Et-$Fl^+$ in nonaqueous acetonitrile was monitored by the appearance of the Et-$Fl^{2+}$ absorption band at 275, 440, and 500 nm. In the case of $Acr^+$, no clear evidence for the formation of $Acr^{2+}$ could be obtained (Figure 10a). Anodic oxidation of $Acr^+$ in the absence of water exhibited a slow decrease of the $Acr^+$ bands at 425 nm. Even after 2 min of controlled potential electrolysis at 2.1 V vs $Ag/Ag^+$, more than 60% of the initial $Acr^+$ absorption was still observed. This behavior is in sharp contrast to Et-$Fl^+$,[59] where most of the Et-$Fl^+$ absorption decayed within 1 min of electrolysis under identical experimental conditions. We attribute this behavior to the fact that $k_{cat}$ = 10 $s^{-1}$ for $Acr^+$ is 10 times larger than $k_{cat}$ = 1 $s^{-1}$ for Et-$Fl^+$. The higher rate of catalysis causes faster recovery of $Acr^+$, giving the appearance of slower decay of its absorption bands. For the same reason, no identifiable absorption bands for oxidized $Acr^{2+}$ were observed, even though a weak shoulder can be observed in the 500−650 nm range (Figure 10a).

Previous studies on Et-$Fl^+$ indicated that oxidized Et-$Fl^{2+}$ reacts with water to form a hydroxylated Et-$FlOH^+$ derivative.[59] In this study, spectroelectrochemical analysis of $Acr^+$ oxidation in the presence of water did not reveal the formation of an analogous $AcrOH^+$ derivative (Figure 10b). The oxidation leads to a decrease of $Acr^+$ absorption bands at 370 and 425 nm without the appearance of any new absorption bands in the visible range. To identify the spectroscopic signature of $AcrOH^+$, chemical oxidation of AcrOH was performed in the presence of Cu(II) ions (Figure 10d). The oxidation generated $AcrOH^+$ with the absorption band in the 600−800 nm range, which is qualitatively similar to the previously reported absorption of the triphenylamine radical cation.[79] Since anodic oxidation of $Acr^+$ in the presence of water does not exhibit detectable absorption in the 600−800 nm range, we conclude that the $AcrOH^+$ ion is not formed.

Two possible scenarios could explain the observed lack of $AcrOH^+$ formation. One explanation is that the pseudobase $pK_a$ value for the formation of AcrOH ($pK_a$ = 11, Figure 1) is much

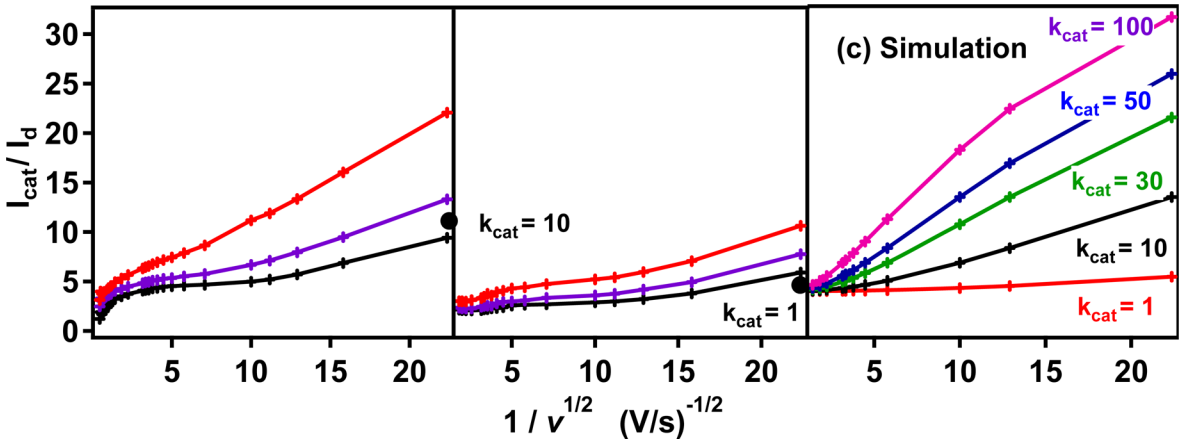


**Figure 9.** Experimental and simulated $I_{cat}/I_d$ values vs $\nu^{-1/2}$ for 1.5 mM $Acr^+$ (panel a) and Et-$Fl^+$ (panel b) on Pt electrode in acetonitrile and 450 mM water (pH = 2 for Et-$Fl^+$ and pH = 7 for $Acr^+$) solution at different potentials: 2.1 V (black), 2.3 V (purple), 2.5 V (red).


dx.doi.org/10.1021/cs5005135 | ACS Catal. 2014, 4, 2635−2644

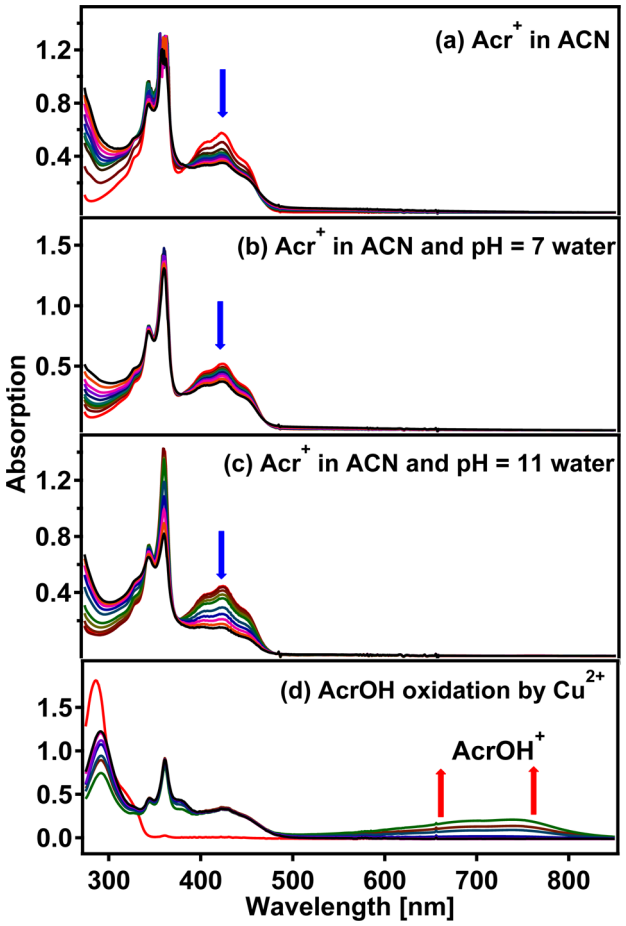


**Figure 10.** UV−vis spectra collected upon electrochemical oxidation of (a) 2 mM $Acr^+$ at 2.4 V vs $Ag/Ag^+$ in acetonitrile; (b) 2 mM $Acr^+$ in acetonitrile with 20 M pH 7 water at 2.4 V vs $Ag/Ag^+$; (c) 2 mM $Acr^+$ in acetonitrile with 20 M pH 11 water at 2.4 V vs $Ag/Ag^+$, 0 (red), 2 (brown), 5 (lime green), 10 (green), 17 (light blue), 30 (dark blue), 45 (purple), 60 (pink), 75 (orange), and 90 s (black); (d) UV−vis absorption changes upon chemical oxidation of 1 mM AcrOH using 1.5 mM $Cu(ClO_4)_2{\cdot}6H_2O$, 0 (red), 2 (brown), 5 (lime green), 10 (green), 17 (light blue), 30 (dark blue), 45 (purple), 60 (pink), and 75 s (black).

higher than the pseudobase $pK_a$ for the formation of Et-FlOH ($pK_a$ = 3.5).[59] To investigate whether $AcrOH^+$formation occurs at higher pH values, the anodic oxidation of $Acr^+$ was performed in the presence of pH = 11 water. Since the formation of $AcrOH^+$ was not observed (Figure 10c), we conclude that the difference in pseudobase $pK_a$ values cannot be used to explain the lack of $AcrOH^+$ formation.

The second explanation for the lack of $AcrOH^+$ formation involves the fact that $k_{cat}$ for $Acr^+$ in the absence of water is 10 times higher than $k_{cat}$ for $Et\text{-}Fl^+$. This high rate of electrocatalysis by $Acr^{2+}$ quickly regenerates $Acr^+$ and does not provide sufficient time for $Acr^{2+}$ to react with water and generate detectable amounts of $AcrOH^+$. We postulate that the lack of $AcrOH^+$ formation and the absence of electrocatalytic water oxidation by $Acr^+$ are due to a high rate of electrochemical process catalyzed by $Acr^+$ in the absence of water. The following section proposes the chemical origin for this electrocatalytic process.

*3.5. Possible Reasons for Different Behaviors of $Acr^+$ and $EtFl^+$.* Two important conclusions can be drawn from the experimental data presented above: (i) Despite significant structural differences between $Acr^+$ and $Et\text{-}Fl^+$, both model compounds exhibit a noticeable current increase at potentials above +1.9 V, and the intensity of this current is strongly dependent on the working electrode material. (ii) The electrocatalytic water oxidation was observed only in the presence of $Et\text{-}Fl^+$, while $Acr^+$ electrochemistry was not affected by the introduction of water. On the basis of these findings, we conclude that electrocatalysis by $Et\text{-}Fl^+$ involves two important processes, one of which is the interaction of the iminium ion with the electrode surface. This interaction is strongly surface-dependent and gives rise to the current at potentials above +1.9 V. The structurally simpler $Acr^+$ model preserves this behavior. The second process involves the electrocatalytic oxidation of water, and this important aspect is not preserved in the $Acr^+$ model.

Our experimental data do not provide sufficient information on what is the cause of a current increase observed for both iminium ions in acetonitrile. One possible explanation is that $Acr^+$ and $Et\text{-}Fl^+$ catalyze a certain electrochemical process and that this process does not involve water molecules. Since amine radical cations tend to perform H atom abstractions efficiently,[80,81] the electrochemical process in question could be the H atom abstraction by oxidized iminium ions from hydroxylated electrode surface (S−OH → S−O + H) or, alternatively, from the solvent ($CH_3CN \rightarrow H^{\bullet} + {}^{\bullet}CH_2CN$). The process would be monomolecular with respect to $Acr^+$, as observed using the concentration-dependent experiments (Figure 4), and the rate of H atom abstraction would be $k_{cat}$ = 10 $s^{-1}$, as obtained using the scan-rate dependent experiments (Figure 9). Furthermore, the process would not be affected by the addition of water. Our attempts to characterize the oxidized products of acetonitrile (such as succinonitrile) after bulk electrolysis were not successful, as no product was detectable by $^1H$ NMR.

The second possible explanation for the observed current increase at potentials above +1.9 V could be the adsorption/desorption of iminium ions to/from the electrode surface. For example, it is known that oxidative or reductive adsorption and desorption occurs efficiently in some classes of organic compounds, such as thiols.[82,83] In the case of $Acr^+$ and $Et\text{-}Fl^+$, the increase in the current could be due to oxidation of the adsorbed iminium ion on the electrode's surface. The lack of the return peak during the cathodic scan can be explained by desorption of the iminium ion after oxidation. In the case of $Et\text{-}Fl^+$, the adsorbed iminium ion film catalyzes the water oxidation, while the adsorbed $Acr^+$ film exhibits no catalytic behavior. Our future experiments will investigate the electrochemical adsorption/desorption of $Et\text{-}Fl^+$ and $Acr^+$ in more detail.

It is generally considered that molecular catalysts offer mechanistic insights into the water oxidation mechanism by their heterogeneous analogs. While transition-metal homogeneous catalysts mimic the catalysis by heterogeneous metal oxides, the organic iminium ions presented here are the model systems for water oxidation by N-doped graphene electrocatalysts.[84] The N-doped carbon-based materials have been extensively investigated for electrocatalytic oxygen reduction,[85−87] and more recently for the reverse reaction, the electrocatalytic water oxidation.[84,88,89] The studies of water oxidation by N-doped graphene have identified pyridinic and quarternary nitrogen centers as the crucial components of the catalytic site,[89−91] but a detailed understanding of the mechanism is lacking due to the difficulties associated with


dx.doi.org/10.1021/cs5005135 | ACS Catal. 2014, 4, 2635−2644

the identification of the intermediates formed at the heterogeneous catalyst. We anticipate that the studies of well-defined molecular systems, such as iminium ions presented here, will provide useful insights into electrocatalytic water oxidation by N-doped graphitic materials.

## CONCLUSIONS

The electrochemical behavior of two iminium ions ($Acr^+$ and Et-$Fl^+$) was investigated for their ability to facilitate catalytic water oxidation process. Cyclic voltammograms of $Acr^+$ and Et-$Fl^+$ in acetonitrile are qualitatively similar: the current increase is observed at potentials above +1.9 V vs $Ag/Ag^+$, and the process is electrode dependent, which suggests an inner-sphere electron transfer mechanism. Further study of concentration dependence suggests that the current depends linearly on iminium ion concentrations. The current increase is assigned to either an electrocatalytic process that does not involve water or the oxidation-induced adsorption/desorption of iminium ion to/from the electrode surface.

Significant differences between $Acr^+$ and Et-$Fl^+$ were observed in the presence of water. The Et-$Fl^+$ catalytic current increases with the addition of water, and the oxygen evolution is detected in the headspace of the cell, suggesting that Et-$Fl^+$ facilitates the electrocatalytic water oxidation. On the other hand, the catalytic current of $Acr^+$ is not affected by the water presence, suggesting that only Et-$Fl^+$ catalyzes water oxidation to molecular oxygen.

The presented molecular systems will likely serve as models for electrocatalytic water oxidation by nitrogen-doped graphitic materials.

## ASSOCIATED CONTENT

### Supporting Information

Experimental procedures, computational methodology, supplementary electrochemical data and results, detailed procedure for electrochemical simulations. This material is available free of charge via the Internet at http://pubs.acs.org.

## AUTHOR INFORMATION

### Corresponding Author

*E-mail: kglusac@bgsu.edu.

### Notes

The authors declare no competing financial interest.

## ACKNOWLEDGMENTS

This work was supported by National Science Foundation (CHE-1055397 to K. D. G and DMR-1212842 to C. M. H.). Computational support from the Ohio Supercomputer Center is gratefully acknowledged.

## REFERENCES

(1) Dau, H.; Limberg, C.; Reier, T.; Risch, M.; Roggan, S.; Strasser, P. *ChemCatChem.* **2010**, *2*, 724−761.
(2) Rüttinger, W.; Dismukes, G. C. *Chem. Rev.* **1997**, *97*, 1−24.
(3) Limburg, B.; Bouwman, E.; Bonnet, S. *Coord. Chem. Rev.* **2012**, *256*, 1451−1467.
(4) Sala, X.; Romero, I.; Rodríguez, M.; Escriche, L.; Llobet, A. *Angew. Chem., Int. Ed.* **2009**, *48*, 2842−2852.
(5) Cady, C. W.; Crabtree, R. H.; Brudvig, G. W. *Coord. Chem. Rev.* **2008**, *252*, 444−455.
(6) Betley, T. A.; Wu, Q.; Van Voorhis, T.; Nocera, D. G. *Inorg. Chem.* **2008**, *47*, 1849−1861.
(7) Gray, H. B. *Nat. Chem.* **2009**, *1*, 7−7.
(8) Lewis, N. S.; Nocera, D. G. *Proc. Natl. Acad. Sci. U. S.A.* **2006**, *103*, 15729−15735.
(9) Gagliardi, C. J.; Vannucci, A. K.; Concepcion, J. J.; Chen, Z.; Meyer, T. J. *Energy Environ. Sci.* **2012**, *5*, 7704−7717.
(10) Rossmeisl, J.; Logadottir, A.; Nørskov, J. K. *Chem. Phys.* **2005**, *319*, 178−184.
(11) Yin, Q.; Tan, J. M.; Besson, C.; Geletii, Y. V.; Musaev, D. G.; Kuznetsov, A. E.; Luo, Z.; Hardcastle, K. I.; Hill, C. L. *Science* **2010**, *328*, 342−345.
(12) Kanan, M. W.; Nocera, D. G. *Science* **2008**, *321*, 1072−1075.
(13) Lutterman, D. A.; Surendranath, Y.; Nocera, D. G. *J. Am. Chem. Soc.* **2009**, *131*, 3838−3839.
(14) Du, P.; Kokhan, O.; Chapman, K. W.; Chupas, P. J.; Tiede, D. M. *J. Am. Chem. Soc.* **2012**, *134*, 11096−11099.
(15) Ellis, W. C.; McDaniel, N. D.; Bernhard, S.; Collins, T. J. *J. Am. Chem. Soc.* **2010**, *132*, 10990−10991.
(16) Fillol, J. L.; Codolà, Z.; Garcia-Bosch, I.; Gómez, L.; Pla, J. J.; Costas, M. *Nat. Chem.* **2011**, *3*, 807−813.
(17) Hong, D.; Murakami, M.; Yamada, Y.; Fukuzumi, S. *Energy Environ. Sci.* **2012**, *5*, 5708−5716.
(18) Blakemore, J. D.; Schley, N. D.; Olack, G. W.; Incarvito, C. D.; Brudvig, G. W.; Crabtree, R. H. *Chem. Sci.* **2010**, *2*, 94−98.
(19) Hocking, R. K.; Brimblecombe, R.; Chang, L.-Y.; Singh, A.; Cheah, M. H.; Glover, C.; Casey, W. H.; Spiccia, L. *Nat. Chem.* **2011**, *3*, 461−466.
(20) Brimblecombe, R.; Swiegers, G. F.; Dismukes, G. C.; Spiccia, L. *Angew. Chem., Int. Ed* **2008**, *47*, 7335−7338.
(21) Limburg, J.; Vrettos, J. S.; Liable-Sands, L. M.; Rheingold, A. L.; Crabtree, R. H.; Brudvig, G. W. *Science* **1999**, *283*, 1524−1527.
(22) Concepcion, J. J.; Jurss, J. W.; Hoertz, P. G.; Meyer, T. J. *Angew. Chem., Int. Ed.* **2009**, *48*, 9473−9476.
(23) Wasylenko, D. J.; Ganesamoorthy, C.; Henderson, M. A.; Koivisto, B. D.; Osthoff, H. D.; Berlinguette, C. P. *J. Am. Chem. Soc.* **2010**, *132*, 16094−16106.
(24) Duan, L.; Bozoglian, F.; Mandal, S.; Stewart, B.; Privalov, T.; Llobet, A.; Sun, L. *Nat. Chem.* **2012**, *4*, 418−423.
(25) Kohl, S. W.; Weiner, L.; Schwartsburd, L.; Konstantinovski, L.; Shimon, L. J.; Ben-David, Y.; Iron, M. A.; Milstein, D. *Science* **2009**, *324*, 74−77.
(26) Gersten, S. W.; Samuels, G. J.; Meyer, T. J. *J. Am. Chem. Soc.* **1982**, *104*, 4029−4030.
(27) Gilbert, J. A.; Eggleston, D. S.; Murphy, W. R., Jr.; Geselowitz, D. A.; Gersten, S. W.; Hodgson, D. J.; Meyer, T. J. *J. Am. Chem. Soc.* **1985**, *107*, 3855−3864.
(28) Liu, F.; Concepcion, J. J.; Jurss, J. W.; Cardolaccia, T.; Templeton, J. L.; Meyer, T. J. *Inorg. Chem.* **2008**, *47*, 1727−1752.
(29) Chronister, C. W.; Binstead, R. A.; Ni, J.; Meyer, T. J. *Inorg. Chem.* **1997**, *36*, 3814−3815.
(30) Hurst, J. K.; Zhou, J.; Lei, Y. *Inorg. Chem.* **1992**, *31*, 1010−1017.
(31) Lei, Y.; Hurst, J. K. *Inorg. Chem.* **1994**, *33*, 4460−4467.
(32) Cape, J. L.; Hurst, J. K. *J. Am. Chem. Soc.* **2008**, *130*, 827−829.
(33) Romain, S.; Bozoglian, F.; Sala, X.; Llobet, A. *J. Am. Chem. Soc.* **2009**, *131*, 2768−2769.
(34) Bozoglian, F.; Romain, S.; Ertem, M. Z.; Todorova, T. K.; Sens, C.; Mola, J.; Rodriguez, M.; Romero, I.; Benet-Buchholz, J.; Fontrodona, X. *J. Am. Chem. Soc.* **2009**, *131*, 15176−15187.
(35) Zong, R.; Thummel, R. P. *J. Am. Chem. Soc.* **2005**, *127*, 12802−12803.
(36) Tseng, H.-W.; Zong, R.; Muckerman, J. T.; Thummel, R. *Inorg. Chem.* **2008**, *47*, 11763−11773.
(37) Concepcion, J. J.; Jurss, J. W.; Brennaman, M. K.; Hoertz, P. G.; Patrocinio, A. O. v. T.; Murakami Iha, N. Y.; Templeton, J. L.; Meyer, T. J. *Acc. Chem. Res.* **2009**, *42*, 1954−1965.
(38) Concepcion, J. J.; Jurss, J. W.; Templeton, J. L.; Meyer, T. J. *J. Am. Chem. Soc.* **2008**, *130*, 16462−16463.
(39) Concepcion, J. J.; Tsai, M.-K.; Muckerman, J. T.; Meyer, T. J. *J. Am. Chem. Soc.* **2010**, *132*, 1545−1557.
(40) Duan, L.; Fischer, A.; Xu, Y.; Sun, L. *J. Am. Chem. Soc.* **2009**, *131*, 10397−10399.

(41) Nyhlén, J.; Duan, L.; Åkermark, B.; Sun, L.; Privalov, T. *Angew. Chem.* **2010**, *122*, 1817−1821.
(42) McDaniel, N. D.; Coughlin, F. J.; Tinker, L. L.; Bernhard, S. *J. Am. Chem. Soc.* **2008**, *130*, 210−217.
(43) Hull, J. F.; Balcells, D.; Blakemore, J. D.; Incarvito, C. D.; Eisenstein, O.; Brudvig, G. W.; Crabtree, R. H. *J. Am. Chem. Soc.* **2009**, *131*, 8730−8731.
(44) Blakemore, J. D.; Schley, N. D.; Balcells, D.; Hull, J. F.; Olack, G. W.; Incarvito, C. D.; Eisenstein, O.; Brudvig, G. W.; Crabtree, R. H. *J. Am. Chem. Soc.* **2010**, *132*, 16017−16029.
(45) Schley, N. D.; Blakemore, J. D.; Subbaiyan, N. K.; Incarvito, C. D.; D'Souza, F.; Crabtree, R. H.; Brudvig, G. W. *J. Am. Chem. Soc.* **2011**, *133*, 10473−10481.
(46) Grotjahn, D. B.; Brown, D. B.; Martin, J. K.; Marelius, D. C.; Abadjian, M.-C.; Tran, H. N.; Kalyuzhny, G.; Vecchio, K. S.; Specht, Z. G.; Cortes-Llamas, S. A. *J. Am. Chem. Soc.* **2011**, *133*, 19024−19027.
(47) Hintermair, U.; Hashmi, S. M.; Elimelech, M.; Crabtree, R. H. *J. Am. Chem. Soc.* **2012**, *134*, 9785−9795.
(48) Carrell, T. G.; Bourles, E.; Lin, M.; Dismukes, G. C. *Inorg. Chem.* **2003**, *42*, 2849−2858.
(49) Limburg, J.; Brudvig, G. W.; Crabtree, R. H. *J. Am. Chem. Soc.* **1997**, *119*, 2761−2762.
(50) Shimazaki, Y.; Nagano, T.; Takesue, H.; Ye, B. H.; Tani, F.; Naruta, Y. *Angew. Chem.* **2004**, *43*, 98−100.
(51) Karlsson, E. A.; Lee, B. L.; Åkermark, T.; Johnston, E. V.; Kärkäs, M. D.; Sun, J.; Hansson, Ö.; Bäckvall, J. E.; Åkermark, B. *Angew. Chem.* **2011**, *123*, 11919−11922.
(52) McCool, N. S.; Robinson, D. M.; Sheats, J. E.; Dismukes, G. C. *J. Am. Chem. Soc.* **2011**, *133*, 11446−11449.
(53) Gerken, J. B.; McAlpin, J. G.; Chen, J. Y.; Rigsby, M. L.; Casey, W. H.; Britt, R. D.; Stahl, S. S. *J. Am. Chem. Soc.* **2011**, *133*, 14431−14442.
(54) Surendranath, Y.; Dinca, M.; Nocera, D. G. *J. Am. Chem. Soc.* **2009**, *131*, 2615−2620.
(55) Chen, Z.; Meyer, T. J. *Angew. Chem., Int. Ed.* **2013**, *125*, 728−731.
(56) Barnett, S. M.; Goldberg, K. I.; Mayer, J. M. *Nat. Chem.* **2012**, *4*, 498−502.
(57) Sichula, V.; Hu, Y.; Mirzakulova, E.; Manzer, S. F.; Vyas, S.; Hadad, C. M.; Glusac, K. D. *J. Phys. Chem. B* **2010**, *114*, 9452−9461.
(58) Sichula, V.; Kucheryavy, P.; Khatmullin, R.; Hu, Y.; Mirzakulova, E.; Vyas, S.; Manzer, S. F.; Hadad, C. M.; Glusac, K. D. *J. Phys. Chem. A* **2010**, *114*, 12138−12147.
(59) Mirzakulova, E.; Khatmullin, R.; Walpita, J.; Corrigan, T.; Vargas-Barbosa, N. M.; Vyas, S.; Oottikkal, S.; Manzer, S. F.; Hadad, C. M.; Glusac, K. D. *Nat. Chem.* **2012**, *4*, 794−801.
(60) Pavlishchuk, V. V.; Addison, A. W. *Inorg. Chim. Acta* **2000**, *298*, 97−102.
(61) Becke, A. D. *J. Chem. Phys.* **1993**, *98*, 5648−5652.
(62) Lee, C.; Yang, W.; Parr, R. G. *Phys. Rev. B* **1988**, *37*, 785−789.
(63) Frisch, M.; Trucks, G.; Schlegel, H. B.; Scuseria, G.; Robb, M.; Cheeseman, J.; Scalmani, G.; Barone, V.; Mennucci, B.; Petersson, G. *Gaussian 09*; Gaussian Inc.: Wallingford, CT, 2009.
(64) Barone, V.; Cossi, M. *J. Phys. Chem. A* **1998**, *102*, 1995−2001.
(65) Anne, A.; Fraoua, S.; Hapiot, P.; Moiroux, J.; Saveant, J. M. *J. Am. Chem. Soc.* **1995**, *117*, 7412−7421.
(66) Panizza, M.; Cerisola, G. *Chem. Rev.* **2009**, *109*, 6541−6569.
(67) Bard, A. J. *J. Am. Chem. Soc.* **2010**, *132*, 7559−7567.
(68) Xin, Y.; Walpita, J.; Zhou, D.; Luk, H. L.; Vyas, S.; Khnayzer, R. S.; Tiwari, S. C.; Diri, K.; Hadad, C. M.; Castellano, F. N. *J. Phys. Chem. B* **2013**, *117*, 15290−15296.
(69) He, Y.; Ye, T.; Borguet, E. *J. Am. Chem. Soc.* **2002**, *124*, 11964−11970.
(70) Lipkowski, J.; Stolberg, L.; Yang, D.-F.; Pettinger, B.; Mirwald, S.; Henglein, F.; Kolb, D. *Electrochim. Acta* **1994**, *39*, 1045−1056.
(71) Kunitake, M.; Akiba, U.; Batina, N.; Itaya, K. *Langmuir* **1997**, *13*, 1607−1615.
(72) Brolo, A.; Jiang, Z.; Irish, D. *J. Electroanal. Chem.* **2003**, *547*, 163−172.
(73) Jurss, J. W.; Concepcion, J. C.; Norris, M. R.; Templeton, J. L.; Meyer, T. J. *Inorg. Chem.* **2010**, *49*, 3980−3982.
(74) Simonson, L.; Murray, R. W. *Anal. Chem.* **1975**, *47*, 290−294.
(75) Jerkiewicz, G.; Vatankhah, G.; Lessard, J.; Soriaga, M. P.; Park, Y.-S. *Electrochim. Acta* **2004**, *49*, 1451−1459.
(76) Nicholson, R. S.; Shain, I. *Anal. Chem.* **1964**, *36*, 706.
(77) Chen, Z.; Concepcion, J. J.; Luo, H.; Hull, J. F.; Paul, A.; Meyer, T. J. *J. Am. Chem. Soc.* **2010**, *132*, 17670−17673.
(78) Wasylenko, D. J.; Palmer, R. D.; Schott, E.; Berlinguette, C. P. *Chem. Commun.* **2012**, *48*, 2107−2109.
(79) Sreenath, K.; Suneesh, C. V.; Ratheesh Kumar, V. K.; Gopidas, K. R. *J. Org. Chem.* **2008**, *73*, 3245−3251.
(80) Simon, S.; Sodupe, M.; Bertran, J. *Theor. Chem. Acc.* **2004**, *111*, 217−222.
(81) Nielsen, M. L.; Budnik, B. A.; Haselmann, K. F.; Olsen, J. V.; Zubarev, R. A. *Chem. Phys. Lett.* **2000**, *330*, 558−562.
(82) Paik, W.-k.; Eu, S.; Lee, K.; Chon, S.; Kim, M. *Langmuir* **2000**, *16*, 10198−10205.
(83) Brett, C.; Kresak, S.; Hianik, T.; Oliveira Brett, A. M. *Electroanalysis* **2003**, *15*, 557−565.
(84) Zhao, Y.; Nakamura, R.; Kamiya, K.; Nakanishi, S.; Hashimoto, K. *Nat. Commun.* **2013**, *4*, 2390.
(85) Gong, K.; Du, F.; Xia, Z.; Durstock, M.; Dai, L. *Science* **2009**, *323*, 760−764.
(86) Zhao, Y.; Watanabe, K.; Hashimoto, K. *J. Am. Chem. Soc.* **2012**, *134*, 19528−19531.
(87) Rao, C. V.; Cabrera, C. R.; Ishikawa, Y. *J. Phys. Chem. Lett.* **2010**, *1*, 2622−2627.
(88) Du, J.; Lai, X.; Yang, N.; Zhai, J.; Kisailus, D.; Su, F.; Wang, D.; Jiang, L. *ACS Nano* **2010**, *5*, 590−596.
(89) Chen, S.; Duan, J.; Jaroniec, M.; Qiao, S. Z. *Angew. Chem.* **2013**, *52*, 13567−13570.
(90) Xue, Y.; Liu, J.; Chen, H.; Wang, R.; Li, D.; Qu, J.; Dai, L. *Angew. Chem.* **2012**, *51*, 12124−12127.
(91) Wang, X.; Li, X.; Zhang, L.; Yoon, Y.; Weber, P. K.; Wang, H.; Guo, J.; Dai, H. *Science* **2009**, *324*, 768−771.